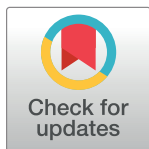


RESEARCH ARTICLE

Modelling extracellular matrix and cellular contributions to whole muscle mechanics

Ryan N. Konno^{1*}, Nilima Nigam¹, James M. Wakeling^{1,2}

1 Department of Mathematics, Simon Fraser University, Burnaby, British Columbia, Canada, **2** Department of Biomedical Physiology and Kinesiology, Simon Fraser University, Burnaby, British Columbia, Canada

* rkonno@sfu.ca

Abstract

Skeletal muscle tissue has a highly complex and heterogeneous structure comprising several physical length scales. In the simplest model of muscle tissue, it can be represented as a one dimensional nonlinear spring in the direction of muscle fibres. However, at the finest level, muscle tissue includes a complex network of collagen fibres, actin and myosin proteins, and other cellular materials. This study shall derive an intermediate physical model which encapsulates the major contributions of the muscle components to the elastic response apart from activation-related along-fibre responses. The micro-mechanical factors in skeletal muscle tissue (eg. connective tissue, fluid, and fibres) can be homogenized into one material aggregate that will capture the behaviour of the combination of material components. In order to do this, the corresponding volume fractions for each type of material need to be determined by comparing the stress-strain relationship for a volume containing each material. This results in a model that accounts for the micro-mechanical features found in muscle and can therefore be used to analyze effects of neuro-muscular diseases such as cerebral palsy or muscular dystrophies. The purpose of this study is to construct a model of muscle tissue that, through choosing the correct material parameters based on experimental data, will accurately capture the mechanical behaviour of whole muscle. This model is then used to look at the impacts of the bulk modulus and material parameters on muscle deformation and strain energy-density distributions.

OPEN ACCESS

Citation: Konno RN, Nigam N, Wakeling JM (2021) Modelling extracellular matrix and cellular contributions to whole muscle mechanics. PLoS ONE 16(4): e0249601. <https://doi.org/10.1371/journal.pone.0249601>

Editor: Jose Manuel Garcia Aznar, University of Zaragoza, SPAIN

Received: November 28, 2020

Accepted: March 19, 2021

Published: April 2, 2021

Copyright: © 2021 Konno et al. This is an open access article distributed under the terms of the [Creative Commons Attribution License](https://creativecommons.org/licenses/by/4.0/), which permits unrestricted use, distribution, and reproduction in any medium, provided the original author and source are credited.

Data Availability Statement: All relevant data are within the paper.

Funding: This work was supported by the Natural Sciences and Engineering Research Council of Canada for Discovery Grants to JW and NN. The funders had no role in study design, data collection and analysis, decision to publish, or preparation of the manuscript.

Competing interests: The authors have declared that no competing interests exist.

Introduction

Skeletal muscle is a complex heterogeneous structure, and a three dimensional continuum model is required to capture its complete mechanics. One dimensional models have been developed, often to describe whole body movement or inter-muscular dynamics (eg. [1]). However, when examining the mechanics or force production of the muscle these models are not sufficient to understand the complex effects from the heterogeneity or architecture of muscle [2]. In fact, three dimensions are required to fully capture the bulging and deformation seen in skeletal muscle [3]. Therefore, to capture the complex aspects of muscle tissue, these models are typically built using the theory of continuum mechanics and solved using a finite element method [4–9].

Muscle is composed of many components making it a highly heterogeneous structure, and these aspects are typically investigated in micro-mechanical [10–14] and homogenization [15–17] models. The tissue heterogeneity effects are often related to micro-structure [18, 19], and these effects cannot be implemented using a single-scale model. The micro-mechanical components of muscle are those that are visible on a microscopic level and contribute to the mechanical behaviour of muscle tissue. There are many micro-mechanical components of muscle aside from the contractile fibres alone. In particular, muscle consists of connective tissue, fluid, cellular components, and muscle fibres which make it a highly heterogeneous material. Skeletal muscle consists of muscle fibres surrounded by a layer of connective tissue (endomysium), and groups of fibres are bundled together into muscle fascicles by another layer of connective tissue (perimysium). Bundles of fascicles are what composes the muscle volume and is held together with a third layer of connective tissue (epimysium) [18, 19]. The combination of connective tissue layers forms the extra-cellular matrix (ECM) and is typically less than 10% of the muscle volume in healthy muscle [20], however the ECM has been shown to have a large impact on the muscle force development [21]. The reason for this is the high degree of structure found in the ECM along with the stiff collagen fibres, which results in a significant contribution to the passive stiffness of the muscle [19, 22–27].

In order to capture the complex effects of the micro-mechanical factors on a whole muscle level, a principled approach needs to be taken. This procedure will allow for consideration of microscopic properties and their effects on the macroscopic muscle model. The micro-mechanical influences on whole muscle effects have been investigated in many studies (eg. [10–12, 14, 15, 17]). A study by Ceelen et al. [12] developed a micro-mechanical model of skeletal muscle for an analysis of the effect of deformation induced hypoxic damage. Sharafi and Blemker [10] developed a formulation of the micro-mechanical effects for healthy muscle that could be implemented in a macroscopic model. Work by Rhörle et al. [13] produced a multi-scale framework for a continuum mechanical model, and included the effects from motor unit recruitment and allows for analysis of electro-physiological behaviour. These developments however do not allow for simple application to the macroscopic level, and hence studies combining the material effects into a homogenous macroscopic model have been performed [15–17]. By performing these homogenizations, a better understanding of the mechanical properties can be obtained in microscopically altered muscle tissue, such as fibrotic tissue that can result from muscular dystrophies, cerebral palsy, and aging [22, 28].

In this study, a principled approach will be taken to develop an isotropic aggregate material that will give a representation of the micro-mechanical effects that can be modelled on a macroscopic level. This homogenization will take into account two factors: a cellular component including the fibres and other cellular materials, and an ECM component. The cellular materials being considered are both effects from cells external to the muscle fibres (eg. satellite cells, nerve bodies, capillaries), as well as the intracellular effect from the fibres aside from the myofibrils. Parameters can be developed independently, so that volume changing as well as isochoric properties can be modified. Additionally, this model will differ from previous homogenization studies (eg. [15, 17]) by considering a nonlinear Yeoh model [29] for the cellular component. Due to the lack of cellular component data, mechanical properties from the cells in brain grey matter will be chosen given the material is composed of the neuron cell bodies. This gives grey matter a nonlinear isotropic response [30, 31], and since this is a collection of cells and similar to the the model's cellular component, these data will be considered. Any anisotropy typically seen in skeletal muscle will be captured in the one dimensional along-fibre component that takes into account the effects from myofilaments within the muscle fibres, and anisotropy conferred by the ECM. Recent experiments have reported varying muscle volume levels over long contractions [32], and changes in volume have been shown to impact passive muscle tension

[33]. The distribution of strain energy-densities has been shown to allow for a deeper understanding of the underlying physics of skeletal muscle mechanics [34]. Therefore, the purpose of this study is to develop a principled model that can be accurately fit to existing experimental data, and can then be used to develop a greater understanding of muscle mechanics in response to altered micro-mechanical properties. In particular, we will look at the impact of the stiffness, volume fraction, and bulk moduli of the individual components in the model through a comparison to experimental data and strain energy-density distribution analysis.

Model

Continuum mechanical formulation

Continuum mechanics is an effective method to model the physics of biological materials, and is typically used in three dimensional skeletal muscle models [4–6, 13, 15, 17]. To characterize the deformation of a body, Ω_0 , to a new deformed state, Ω , we can introduce the deformation gradient, \mathbf{F} . The deformation gradient can be defined as

$$\mathbf{F} = \frac{d\mathbf{x}}{d\mathbf{X}} \quad (1)$$

where $d\mathbf{X}$ is a line element in the original reference configuration and $d\mathbf{x}$ is a line element in the deformed current configuration. \mathbf{F} contains the information about how the original configuration is deformed, via rotations or stretches, to get to the current configuration. The dilatation of the material can be denoted as $J = \det(\mathbf{F})$, and remains close to 1.

To characterize the response of a material to deformation, the constitutive laws for the material need to be determined. To do this, stress and strain tensors need to be defined. The model developed here will consider the left Cauchy-Green strain tensor $\mathbf{b} = \mathbf{F}\mathbf{F}^T$ to characterize the strain in the material. Skeletal muscle can be modelled using a nonlinear hyperelastic approach. For a hyperelastic material, the formulation of the constitutive relationships can be performed in terms of a strain-energy function which can be calculated at each material point, \mathbf{X} . The strain-energy function can be represented in the reference configuration as $W(\mathbf{X}, \mathbf{b}) \equiv W(\mathbf{b})$. Characterizing the material in terms of the strain-energy allows us to write the constitutive law in terms of the Cauchy Stress Tensor, σ , and the left Cauchy-Green strain tensor,

$$\sigma(\mathbf{b}) = 2J^{-1}\mathbf{b} \frac{\partial W(\mathbf{b})}{\partial \mathbf{b}}. \quad (2)$$

In order to determine the constitutive law explicitly, the exact form of $W(\mathbf{b})$ needs to be determined. For skeletal muscle the strain-energy function can be broken into a volumetric and isochoric component.

$$W_{\text{muscle}} = W_{\text{vol}}(J) + W_{\text{iso}}(\bar{\mathbf{b}}) \quad (3)$$

where $\bar{\mathbf{b}}$ is the isochoric component of the left Cauchy-Green Strain tensor, and is defined as $\bar{\mathbf{b}} = J^{-2/3}\mathbf{b}$. The strain-energy function for skeletal muscle, $W_{\text{muscle}}(\mathbf{b})$, is composed of the three dimensional base material component, $W_{\text{BM}}(\mathbf{b})$, and an along-fibre component, $W_{\text{fibre}}(\lambda)$, which depends on the local fibre stretch ($\lambda = \|\mathbf{F}\mathbf{a}_0\|$) along the direction of the muscle fibres. \mathbf{a}_0 denotes the initial fibre direction with unit length at a given point and $\|(\cdot)\|$

denotes the usual L^2 norm of (\cdot) . Therefore, the volumetric and isochoric components are

$$\begin{aligned} W_{\text{iso}} &= W_{\text{fibre}}(\lambda) + W_{\text{BM,iso}}(\bar{\mathbf{b}}), \\ W_{\text{vol}} &= W_{\text{BM,vol}}(J). \end{aligned} \quad (4)$$

The continuum mechanical formulation developed here can be implemented into a three dimensional finite element model using a three field formulation with the unknowns being the displacement \mathbf{u} , pressure p , and dilation J [35]. The Principle of Stationary Energy can be applied to the problem by taking the first variation of the total energy. This gives a nonlinear problem that can be solved using the finite element library Deal ii [36]. Details on the implementation and finite element method can be found in Domínguez [37] and [S1 Appendix](#).

A principled approach to muscle base material

Formulation of the base material. Muscle is often modelled as a fibre reinforced material [4, 6, 7], and so the model developed in this study will consider the muscle as a three dimensional isotropic material with one dimensional fibres running along the length of the muscle belly. The one dimensional along-fibre component is designed to account for any anisotropic effects in the direction of the muscle fibres. In particular, this includes the passive along-fibre effects from within the sarcomeres, such as from the protein titin, and active forces developed between actin and myosins. To analyze the micro-mechanical properties in whole muscle, the isotropic base material can then be constructed by combining the effects from the principle components (ECM and cellular materials). Since the base material has both isochoric and volumetric parts, the a homogenization will need to occur in both of these strain-energy components.

The base material can be formulated by considering a representative volume element (RVE) that encompasses a region, V_{RVE} , in the initial reference configuration. Since the RVE consists of each of the micro-mechanical components of the muscle, a portion of it will consist of ECM, V_{ECM} . The rest of the volume will consist of the cellular component, V_{cell} . Let $|V_{\text{RVE}}|$ denote the volume the region V_{RVE} , then the volume fraction of each material can be defined as

$$\frac{|V_{\text{ECM}}|}{|V_{\text{RVE}}|} = \alpha, \quad \frac{|V_{\text{cell}}|}{|V_{\text{RVE}}|} = 1 - \alpha. \quad (5)$$

The volume fractions, α and $1 - \alpha$, are determined in the reference configuration of the RVE, and we assume these volume fractions do not change as the muscle deforms. Since skeletal muscle achieves near incompressibility, this is an accurate approximation to leading order.

The total energy of the RVE, E_{RVE} , can be written in terms of the microscopic strain-energy functions for the ECM and cellular components as

$$\begin{aligned} E_{\text{RVE}}(\mathbf{b}) &= \int_{V_{\text{RVE}}} W_{\text{RVE}}(\mathbf{b}) dV \\ &= \int_{V_{\text{ECM}}} s_{\text{ECM}} W_{\text{ECM,RVE}}(\mathbf{b}) dV + \int_{V_{\text{CELL}}} W_{\text{CELL,RVE}}(\mathbf{b}) dV \end{aligned} \quad (6)$$

where s_{ECM} is a structural area parameter that is constant over the RVE and will be discussed

in more detail in the next section. Dividing by $|V_{RVE}|$ gives

$$\begin{aligned} \frac{1}{|V_{RVE}|} \int_{V_{RVE}} W_{RVE}(\mathbf{b}) dV &= \frac{1}{|V_{RVE}|} \int_{V_{ECM}} s_{ECM} W_{ECM,RVE}(\mathbf{b}) dV \\ &+ \frac{1}{|V_{RVE}|} \int_{V_{CELL}} W_{CELL,RVE}(\mathbf{b}) dV \\ &= \alpha \frac{1}{|V_{ECM}|} \int_{V_{ECM}} s_{ECM} W_{ECM,RVE}(\mathbf{b}) dV \\ &+ (1 - \alpha) \frac{1}{|V_{CELL}|} \int_{V_{CELL}} W_{CELL,RVE}(\mathbf{b}) dV. \end{aligned} \tag{7}$$

Given that the RVE is microscopic in size, the following approximations were made

$$\begin{aligned} W(\mathbf{b}) &\approx \frac{1}{|V_{RVE}|} \int_{V_{RVE}} W_{RVE}(\mathbf{b}) dV \\ W_{ECM}(\mathbf{b}) &\approx \frac{1}{|V_{ECM}|} \int_{V_{ECM}} W_{ECM,RVE}(\mathbf{b}) dV \\ W_{CELL}(\mathbf{b}) &\approx \frac{1}{|V_{CELL}|} \int_{V_{CELL}} W_{CELL,RVE}(\mathbf{b}) dV \end{aligned} \tag{8}$$

where \mathbf{b} denotes the left Cauchy-Green strain tensor at the centroid of the RVE. This is the familiar Voigt approximation used in skeletal muscle homogenization studies [15, 16].

It then follows that the strain-energy function for the macroscopic base material can be written as a linear combination of the strain energies from each component:

$$W_{BM,iso}(\mathbf{b}) = \alpha s_{ECM} W_{ECM}(\mathbf{b}) + (1 - \alpha) W_{cell}(\mathbf{b}). \tag{9}$$

Similarly, it is possible to decompose the volumetric strain-energy function into its micro-mechanical components. The volumetric strain-energy component will be characterized using a strain-energy function typically used for soft biological materials [38], and the aggregate function is given as

$$W_{BM,vol}(J) = \frac{1}{4} (J^2 - 1 - 2 \log(J)) [\alpha \kappa_{ECM} + (1 - \alpha) \kappa_{cell}]. \tag{10}$$

The bulk moduli, κ_{ECM} and κ_{cell} , are parameters that will impact the compressibility of the model and can be varied independently for each component.

Micro-mechanical components. The strain-energy function for the ECM, $W_{ECM}(\mathbf{b})$, can be determined using experimental data from Gillies et al. [39], which obtained stress-strain curves for decellularized skeletal muscle tissue. These data are used as they are the only mechanical data available for the entire ECM. Other micro-mechanical models consider the response from the isotropic component of the ECM to be of the same order of magnitude [15] as that of the fibres, instead, in this model we consider experimental data for the ECM that have been measured for a decellularized matrix. Additional data for the ECM component will allow for a more accurate representation in the model. Due to difficulty in measuring the decellularized cross-sectional area of the ECM, the stress-strain relationship is typically

reported with respect to the cross-sectional area of the muscle tissue. Therefore, to account for this cross-sectional area calculation in the model, the additional coefficient, s_{ECM} , is used.

Material data for the cellular (non-contractile and non-ECM) properties of skeletal muscle are not available. Some studies have been able to measure properties of isolated muscle fibres. However, tensile data are only available for the longitudinal direction of the muscle fibres [40], which may not necessarily represent the response in the transverse direction. Ideally, data for the cellular component of the base material would be tensile data for fibre and other cellular components measured transverse to the fibre orientation. Since these data are not available other data need to be considered, such as the mechanical behavior of brain grey matter or liver tissue. These materials are considered since they are essentially a cellular mass with no collagen fibres and are often modelled as non-linear isotropic materials [30, 31, 41–43]. Along fibre data have been considered in the homogenization models by Bleiler et al. [17] and Spyrou et al. [15], however, they only considered a linear stress-strain response shown by Smith et al. [28]. Since the liver material has been shown to have some anisotropy, which is likely due to micro-structural effects, grey matter is used for the cellular component.

In order to implement the experimental data for the ECM and cellular components into the model a strain-energy function needs to be used for each of the components. The Yeoh model (Eq 11) gives the energy associated with a deformation in terms of the first invariant of $\bar{\mathbf{b}}$ [29].

$$W(\bar{\mathbf{b}}) = c_1(I_1 - 3) + c_2(I_1 - 3)^2 + c_3(I_1 - 3)^3 \tag{11}$$

This provides a computationally simplistic model that can sufficiently capture the isotropic behaviour of these components as demonstrated by r^2 values of 0.998 and 0.999 for the ECM and cellular material, respectively (Fig 1A). Fig 1 illustrates the fit of the model for the intrinsic micro-mechanical properties (ECM and cellular components) used in the model along with the experimental whole muscle data from Mohommadhah et al. [44]. s_{ECM} was set at 200 in Fig 1 to account for the aforementioned cross-sectional area calculation effects. This gives a significantly stiffer curve for the ECM compared to both the whole muscle data and the cellular component (Fig 1(A)), which is expected.

Implementation of the along-fibre component

The along-fibre component of the model was obtained through fitting to experimental data by Winters et al. [45] and is shown in Fig 1(B) in terms of its stress-stretch relationship. The stress response for the passive component of the fibres is given as

$$\sigma_{\text{pass}}(\lambda) = \sigma_0 \begin{cases} 0 & 0 \leq \lambda \leq 1.0 \\ 2.353(\lambda - 1.0)^2 & 1.0 \leq \lambda \leq 1.25 \\ 3.44(\lambda - 1.25)^2 + 1.18(\lambda - 1.25) + 0.147 & 1.25 \leq \lambda \leq 1.5 \\ 0.427(\lambda - 1.5)^2 + 2.90(\lambda - 1.5) + 0.656 & 1.5 \leq \lambda \leq 1.65 \\ 3.023(\lambda - 1.65) + 1.1 & \lambda > 1.65, \end{cases} \tag{12}$$

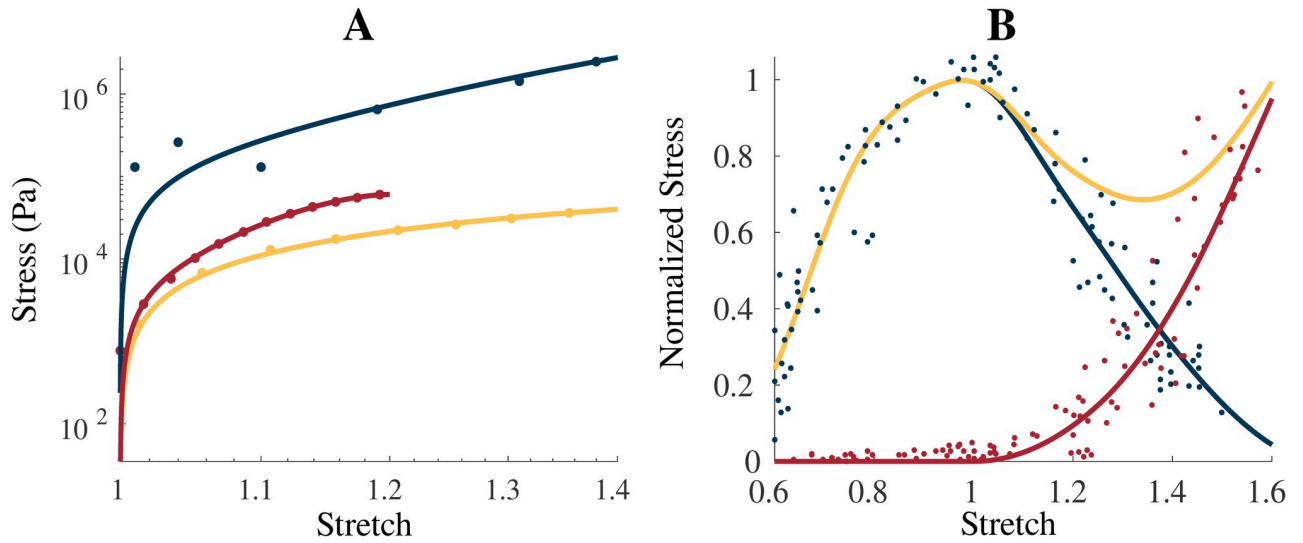


Fig 1. Intrinsic model properties. (A) shows the uniaxial stress-stretch relationship for the intrinsic properties of the homogenization: ECM (blue), cellular (yellow), and averaged whole muscle components (red), along with experimental data from Gillies et al. [39] (ECM, blue dot), Jin et al. [30] (brain grey matter, yellow dot), and Mohammadkhah et al. [44] (transverse muscle response, red dot). The averaged whole muscle component was fit to experimental data and is shown for comparison. Total (yellow), passive (red), and active (blue) stress-stretch relationships are shown for the along-fibre response in (B) with the experimental data obtained by Winters et al. [45] and normalized to $\sigma_0 = 2 \times 10^5$ Pa. ECM component was scaled by 200 in (A) to account for cross-sectional area calculations.

<https://doi.org/10.1371/journal.pone.0249601.g001>

and the active component of the fibres as

$$\sigma_{act}(\lambda) = \begin{cases} \sigma_0 \left(0.642 \sin(1.29\lambda + 0.629) \right. \\ \quad + 0.325 \sin(5.31\lambda - 4.52) \\ \quad + 0.328 \sin(6.74\lambda + 1.69) \\ \quad + 0.015 \sin(19.8\lambda - 7.39) \\ \quad + 0.139 \sin(8.04\lambda + 2.54) \\ \quad + 0.0018 \sin(32.2\lambda - 6.45) \\ \quad \left. + 0.012 \sin(23.2\lambda - 2.64) \right) & \text{if } 0.4 \leq \lambda \leq 1.75 \\ 0 & \text{otherwise.} \end{cases} \quad (13)$$

Here, $\sigma_0 = 2 \times 10^5$ Pa is the maximum isometric stress. The active component in the model is also multiplied by a function $a(t)$ that represents the activation, which increased from 0 to 1 over the course of the contraction. $a(t)$ is linearly ramped in discrete steps t , which we will call “timesteps”. At each step we compute the new state \mathbf{u} , p , and J of the muscle. The relationship between the stress and the strain-energy functions is given by

$$\sigma(\lambda) = \lambda \frac{\partial W(\lambda)}{\partial \lambda}. \quad (14)$$

The strain-energy function for the along-fibre component can then be formulated as

$$W_{fibre}(\lambda) = W_{pass}(\lambda) + a(t)W_{act}(\lambda). \quad (15)$$

Table 1. Summary of parameters used in the model. List of the values for the aforementioned parameters used in this model. $c_{i,cell/ecm}$ are the Yeoh model parameters shown in Eq 11 and were obtained using nonlinear regression analysis.

Parameter	Value/Range of Values
$c_{1,cell}$	3703
$c_{2,cell}$	-707.7
$c_{3,cell}$	123.2
$c_{1,ecm}$	1988
$c_{2,ecm}$	4917
$c_{3,ecm}$	-591.5
α	2–20%
κ_{ECM}	150–250
κ_{cell}	1×10^6 – 1×10^8 Pa
κ_{ECM}	1×10^6 Pa
σ_0	2×10^5 Pa

<https://doi.org/10.1371/journal.pone.0249601.t001>

All of the parameters used in the model, and their values are summarized in Table 1. The base material and along-fibre component were implemented in a quasi-static model described in Wakeling et al. [34].

Methods

Stress-strain experiments

A block of muscle was constructed as seen in Fig 2(A), which had dimensions 20 cm \times 6 cm \times 4 cm. The fibre properties were implemented along the length of the muscle model in the longitudinal direction (parallel to the x axis). To perform stress-strain tests that will allow for a comparison to experimental whole muscle data, the $-x$ face was constrained from movement in x , y , z directions. A traction was then applied to the $+x$ face of the muscle which extended the muscle in the longitudinal direction.

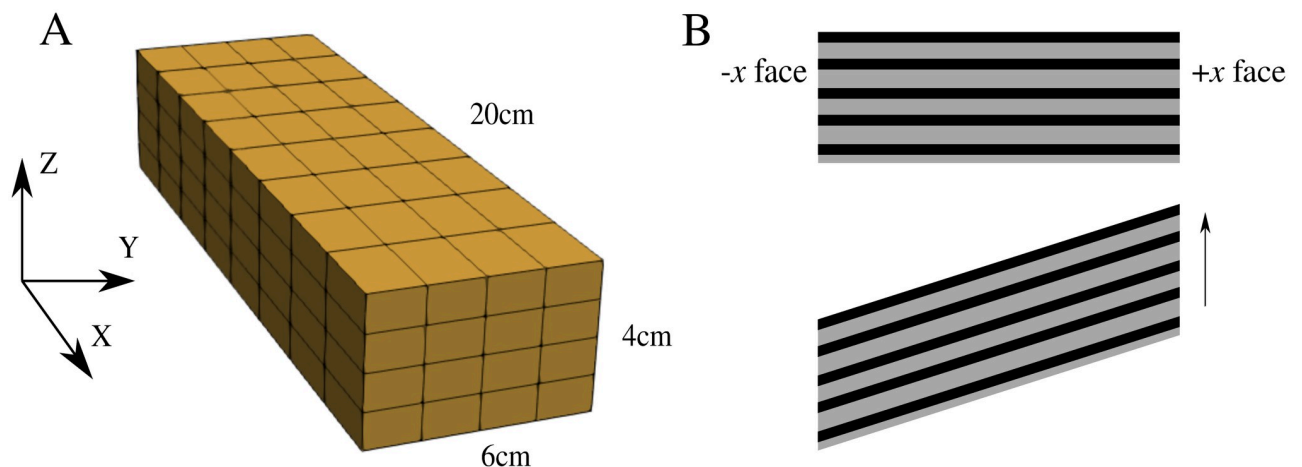


Fig 2. Mesh and experiment setup. (A) Mesh of the geometry used for the numerical experiments. The geometry had dimensions 20cm \times 6cm \times 4cm and muscle fibre properties are orientated along the x axis. (B) Shear experiment setup. The $-x$ face was constrained in all directions, while the $+x$ face was constrained in the x direction only. The arrow represents direction of applied shear stress.

<https://doi.org/10.1371/journal.pone.0249601.g002>

These tests were performed with varying α in the range 0.02–0.20 and s_{ECM} coefficients of 150 and 250. The stiffness coefficients were varied to give results that are comparable to experimental data for muscle. The range from 2% to 10% volume fractions of ECM are typically found in healthy muscle [20, 21], and larger volume fractions in the range of 10% to 20% are found in fibrotic tissue [21]. By comparing the stress-strain curves of the model to experimental data, the accurate homogenization parameters, s_{ECM} and α , can be determined.

Shear experiments

Shear tests were performed to investigate the behaviour of the model in response to more complex deformation modes. A shear stress was applied to the $+x$ face of the model, which was constrained from movement in the x direction. To apply the shear stress to the model, we specify the component of the non-zero traction boundary condition in the y direction and set the x and z component of the traction to 0. Meanwhile, the $-x$ face was constrained in all directions (Fig 2B). The shear stress was applied in three different scenarios to determine the impact of the base material stiffness and anisotropy in the model: (1) the shear stress was applied without activation with $\alpha = 0.05$ and 0.10, (2) the shear stress was applied prior to activation of the model, and (3) the shear stress was applied after activation of the model.

Investigation of bulk modulus and strain-energy properties

Muscle is typically considered to be isovolumetric, however, small changes in volume may occur during muscle stretches [46], and also during long fatiguing contractions [32]. Willwacher et al. [32] found that volume changes occurred up to 9% in the gastrocnemii during running activities, and so to confine volume changes to this range a value for $\kappa > 1 \times 10^6$ Pa is required. Given the results from previous studies and lack of experimental data for the compressibility of the ECM, the κ_{ECM} was left at 1×10^6 Pa [4]. Skeletal muscle consists of 80% water [47], which is contained in the cellular component of the muscle and makes it highly incompressible. Therefore, κ_{cell} was varied in the range 1×10^6 to 1×10^8 Pa to look at the effects of the bulk moduli on the stress-strain relationship and strain energy-density distribution. The micro-mechanical components impact the overall stiffness of the base material component, and these effects on the strain-energy distribution were also investigated with $\kappa_{\text{cell}} = 1 \times 10^7$ Pa, $\kappa_{\text{ECM}} = 1 \times 10^6$ Pa, and $s_{\text{ECM}} = 150$. To obtain a better understanding of the physics occurring in the model, the volume fractions of ECM were varied between 2% and 100%. The set up for these tests was the same as for the tests for the stress-strain experiments with the addition of an activation phase after the passive lengthening. This involved constraining both the positive and negative x faces of the muscle block after the muscle had been passively lengthened, then increasing the activation in the muscle to 100%.

Results

Stress-strain results

The model qualitatively demonstrates similar stress-stretch behaviour to available experimental data. These data for skeletal muscle vary depending on the species [44, 48], so it is not useful to compare directly to one particular set of muscle data. The stress values from the model are the applied traction to the $+x$ face of the block, and the stretch values are the whole muscle stretch

$$\lambda_{\text{muscle}} = \frac{l}{l_0}, \quad (16)$$

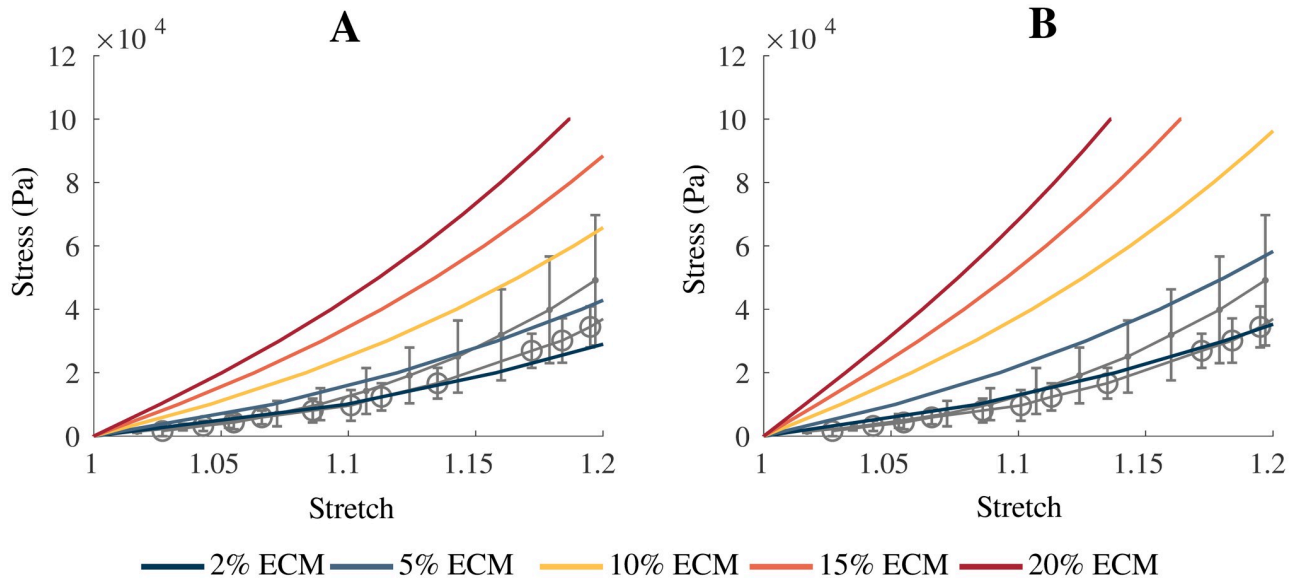


Fig 3. Comparison of model results to experimental data. Comparison of model passive stress-stretch curves to experimental data for skeletal muscle. (A) Gives the model with a parameter of $s_{ECM} = 150$, while (B) is the model with a parameter of $s_{ECM} = 250$. α was varied between 0.02–0.20, which corresponds to 2–20% volume fraction of ECM. The grey lines represent experimental data from Takaza et al. [48] (circle) and Mohammadkhah et al. [44] (dot). Error bars represent \pm standard deviation when available.

<https://doi.org/10.1371/journal.pone.0249601.g003>

where l_0 and l are the initial length and current length of the muscle belly, respectively. Fig 3 shows that for $s_{ECM} = 150$ and 250 there is a particularly good match at smaller stretch values. Comparable material stiffness to healthy muscle occurs for $\alpha < 0.10$ for $s_{ECM} = 150$ which is a larger range of volume fractions compared to $s_{ECM} = 250$ (< 0.05). However, to better capture the nonlinearity seen at larger strains a larger value of $s_{ECM} = 250$ is required. As the volume fraction of the ECM was increased, there was an increase in stiffness that is expected with fibrotic tissue.

Shear results

The effects of applying a shear stress to the model was demonstrated in Fig 4 with shear strain calculated as

$$\epsilon_{\text{shear}} = \frac{\bar{u}_y}{l_0}, \tag{17}$$

where \bar{u}_y is the mean displacement in the y direction of the $+x$ face. At small values of shear strain, there is a linear region in the shear stress-strain relationship and only a small effect from the variation in α (Fig 4). This shows there is more influence from the fibres for small shear stresses. At larger strains, the stress response for the model varies with α , and the graph becomes more nonlinear, demonstrating the nonlinearity in the base material (Fig 1A). While the model is active, shear stress-strain relationship becomes more linear due to larger fibre forces (Fig 4B). In Fig 4(D) and 4(E), the three dimensional mesh of the model is shown at 100% activation. The largest dilations occur in the corners of the model which experience the most stretching during the shear. Fig 4(D) shows the model during a fixed-length contraction after a shear stress has been applied. The deformation and dilation are smaller, compared to Fig 4(E), where the model has been first activated then sheared.

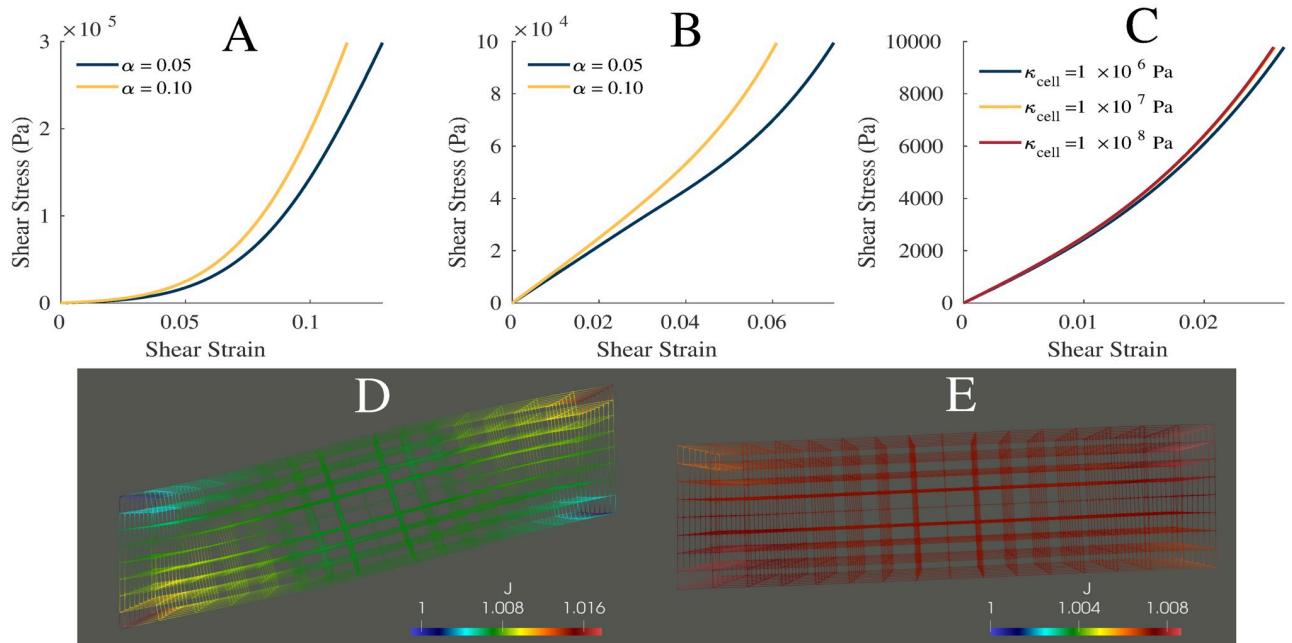


Fig 4. Shear properties. Plot of the shear stress-strain relationship for $\alpha = 0.05, 0.10$ and $s_{ECM} = 250$, while the muscle is passive (A) and active (B). (C) Shear stress-strain relationship for bulk moduli of $1 \times 10^6, 1 \times 10^7$, and 1×10^8 Pa. Wire mesh of muscle model after shear stress was applied then model was activated (D), and after first activation then application of shear stress (E). (D,E) Color represents the dilation seen in the muscle model. (C) Shear stress-strain relationship for bulk moduli of $1 \times 10^6, 1 \times 10^7$, and 1×10^8 Pa.

<https://doi.org/10.1371/journal.pone.0249601.g004>

Volumetric effects

Variation in the bulk modulus of the cellular component shows small effects on the normal stress-strain (Fig 5) and shear stress-strain (Fig 4(C)) relationships. The largest variations in

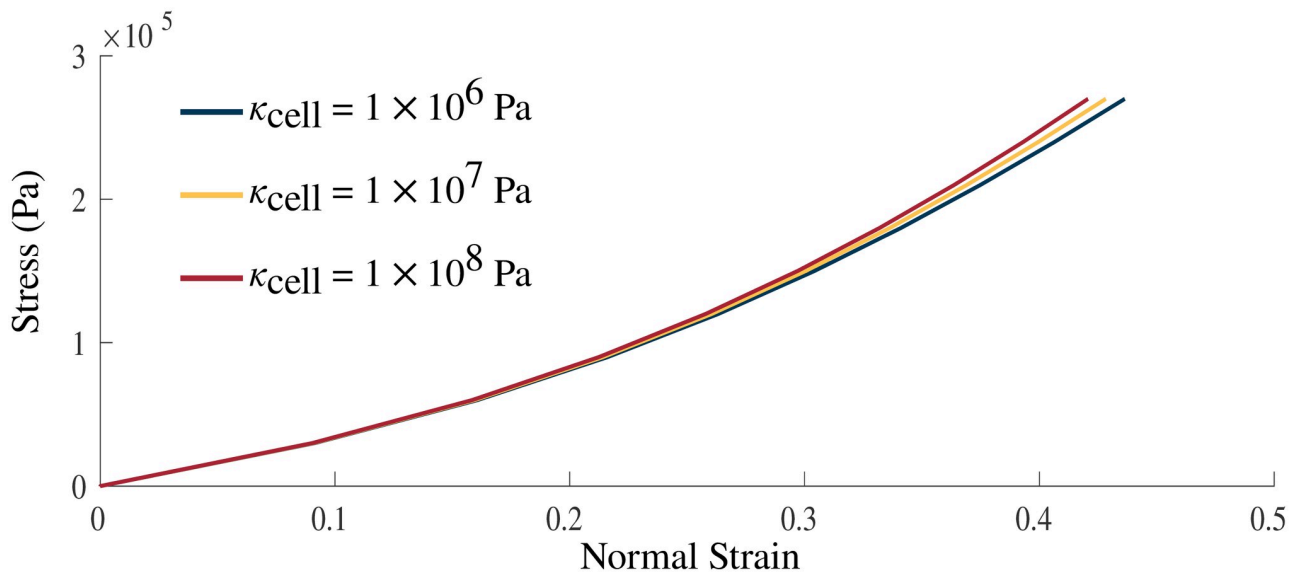


Fig 5. Volumetric impact on stress-strain relationship. Stress-strain relationship with $\kappa_{cell} = 1 \times 10^6, 1 \times 10^7, 1 \times 10^8$ Pa. Stress was applied in the longitudinal direction on the $+x$ face of the muscle model. Increasing values of the bulk moduli result in a stiffer material.

<https://doi.org/10.1371/journal.pone.0249601.g005>

Table 2. Total volume change and normalized stress on the +x face of the muscle after passive lengthening to a stress of 1×10^5 Pa and fixed length contraction to an activation of 100%. The stress was normalized to σ_0 . These values are measured with homogenization parameters of $\alpha = 0.05$ and $s_{ECM} = 250$.

κ_{cell} (Pa)	Volume Change (%)	Normalized Stress at 100% Activation
1×10^6	7.3	0.875
1×10^7	0.8	0.907
1×10^8	0.1	0.912

<https://doi.org/10.1371/journal.pone.0249601.t002>

the stress-strain relationships were observed between $\kappa_{cell} = 1 \times 10^6$ Pa and 1×10^7 Pa whereas smaller variations between the relationships were seen at larger κ_{cell} . Table 2 gives the volume changes and normalized stresses on the +x face of the muscle during the normal stress-strain experiment, where the change in volume was calculated as the ratio between the current volume and initial volume. The volume in its new configuration was calculated as

$$Vol = \int_{V_0} \det(\mathbf{F}) dV_0, \quad (18)$$

where V_0 is the initial configuration of the muscle. At larger bulk moduli smaller changes in volume were seen at maximal activation, for $\kappa_{cell} = 1 \times 10^8$ Pa the change in volume was considerably smaller at 0.1% change in volume compared to the 7.3% change in volume seen for $\kappa_{cell} = 1 \times 10^6$ Pa. While the changes in volume varied substantially, the effect on the total muscle force was small (Table 2).

Changes in the κ of the muscle material also had an impact on the strain energy-density distribution of the model. The strain energy-density calculations were performed as in Wakeling et al. [34]. There was very little change to many of the energy components, in particular, the isochoric components of the energies for the passive lengthening periods of the experiments (Fig 6). There was only a substantial effect to the strain energy-densities in the volumetric component where the energy decreases with increasing bulk moduli. Large effects were seen during activation on the volumetric component with activation increasing the volumetric energy for some values of κ_{cell} (1×10^6 Pa) and decreasing the energy for others ($\kappa_{cell} = 1 \times 10^7$, 1×10^8 Pa). Overall, the total internal energy remains largely unchanged by the value of κ_{cell} .

Micro-mechanical impacts on the strain-energy distribution

Fig 7 shows the impact of varying the volume fraction of ECM in the ranges 2-100% on the strain energy-density distribution during a passive lengthening test and fixed-end contraction. As the volume fraction of the ECM becomes larger the muscle becomes stiffer, smaller strains are reached and less deformation occurs, which then results in smaller magnitudes of energy potentials. The volumetric component of the energy decreases as the stiffness in the material decreases, while the opposite behaviour occurs for each of the other components in the material. Additionally, similar effects are seen during activation to the results in Fig 6, where there is increasing volumetric energy for positive volumetric strain-energies and decreasing volumetric energy for negative volumetric strain-energies. In contrast to variations in the bulk moduli (Fig 6), the total internal energy in the model is affected more by variations in the volume fraction of ECM.

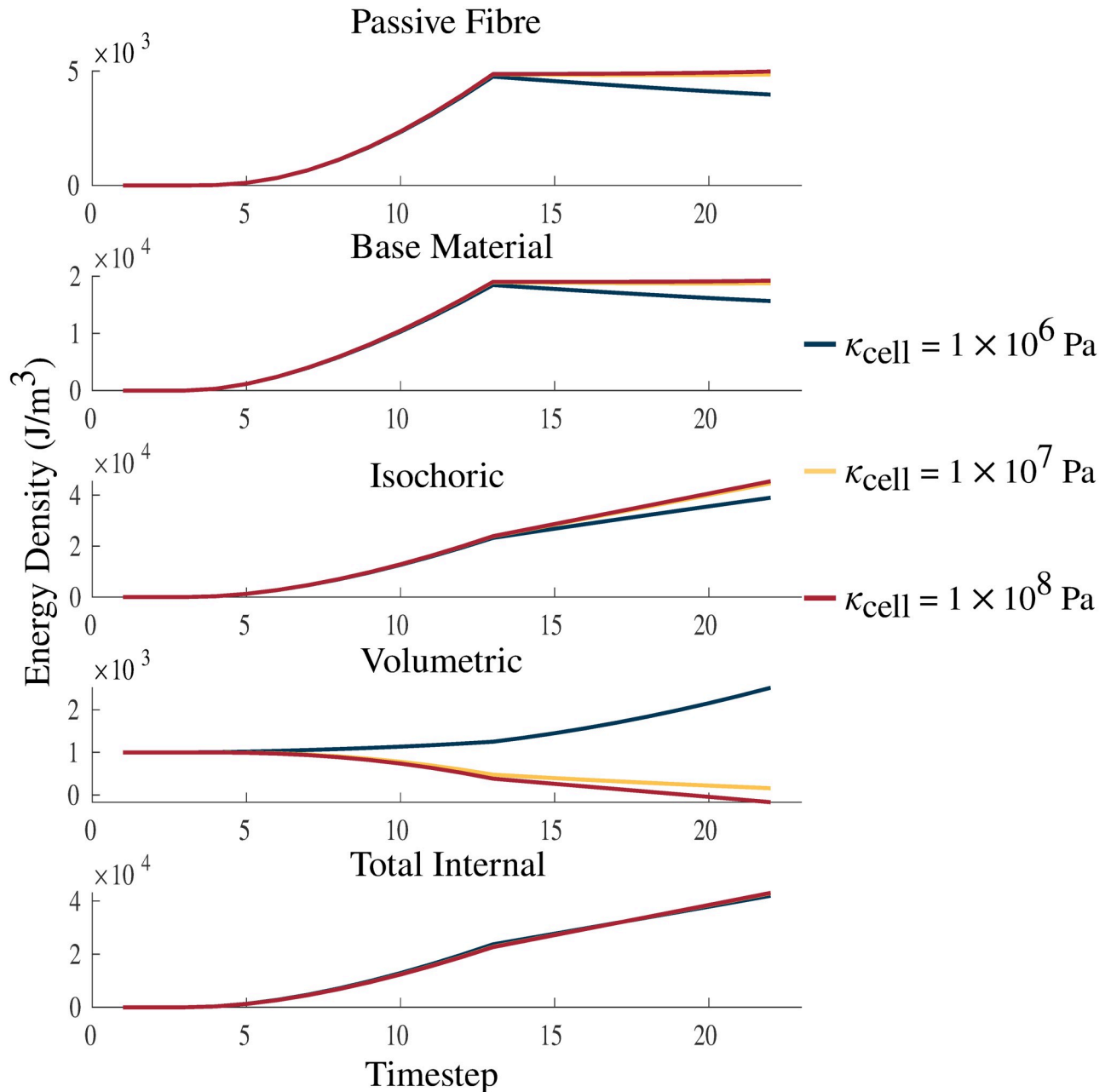


Fig 6. Strain energy-density with varying κ_{cell} . Plots of passive fibre, base material, isochoric, volumetric, and total internal strain energy-densities. The energies are plotted over a passive lengthening period, up to a traction of 1×10^5 Pa, from timestep 3 to 13, and a linearly increasing fixed-length activation from timestep 13 to 23. κ_{cell} is varied between values 1×10^6 Pa, 1×10^7 Pa, and 1×10^8 Pa. The larger values of κ_{cell} demonstrate increasing incompressibility and approach the bulk moduli of water (2.15×10^9 Pa [49]), which is considered to be almost completely incompressible. The total internal strain energy-density is the combination of the volumetric, isochoric, and activation (not shown in figure) energies.

<https://doi.org/10.1371/journal.pone.0249601.g006>

Discussion

Micro-mechanical properties

The approach taken in this study develops a base material for whole muscle based on the principle micro-mechanical components. This aggregate base material is implemented into a continuum mechanical model developed in previous studies [4, 34]. This homogenized base

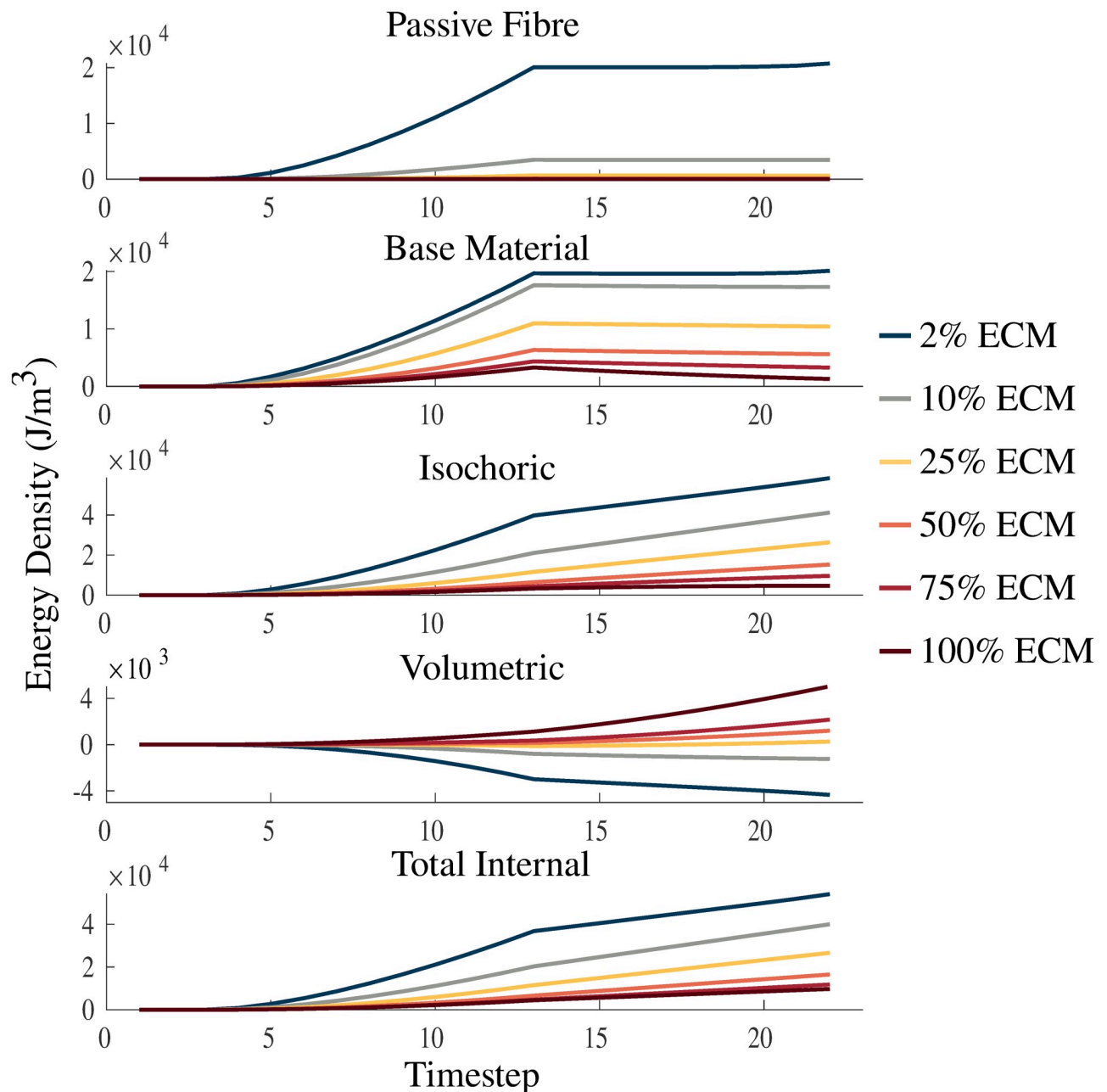


Fig 7. Strain energy-density with varying ECM volume fraction. Plots of passive fibre, base material, isochoric, volumetric, and total internal strain energy-densities. The energies are plotted over a passive lengthening period, up to a traction of 1×10^5 Pa, from timestep 3 to 13, and a linearly increasing fixed-length activation from timestep 13 to 23. Volume fractions of the ECM are varied between 2%, 25%, 50%, 75%, and 100% to investigate the physics of the model.

<https://doi.org/10.1371/journal.pone.0249601.g007>

material showed a good comparison to the experimental data from Takaza et al. [48] and Mohammadkhah et al. [44], with which it was developed. The s_{ECM} parameter was varied to account for uncertainty in the experimental data calculation, however, with improved experimental techniques alteration of s_{ECM} may not be required. As described previously, the larger values of s_{ECM} result in larger nonlinearity in the stress-strain curves for the muscle tissue. This implies the ECM component of the model is largely responsible (along with the

anisotropic component) for the nonlinear effects seen in the model, which agrees with experimental data [18, 28]. Binder-Markey et al. [20] found that the ECM volume fractions for various skeletal muscles were typically less than 10%, and for some muscles (eg. Semimembranosus) the volume fractions were less than 2%. Therefore, the volume fractions less than 10% in Fig 3(A) and less than 5% in Fig 3(B) are reasonable ranges when compared to the experimental data for healthy muscle.

While other models have considered an explicit anisotropic ECM [15–17], in the model developed here these effects are accounted for in the one dimensional along-fibre component. Nevertheless, accurate stress-strain mechanics result from the model (Fig 3). A unique component of this model is the use of a nonlinear cellular component derived from brain grey matter. The cellular component of muscle is difficult to measure experimentally, and grey matter provided a good substitute. It demonstrated similar isotropic effects and structure to the cellular component of muscle, and therefore provided good experimental data for the model. Some homogenization methods have considered a linear titin response for the cellular contribution [15, 17], which may not elicit an isotropic response in muscle, or a response derived through a ratio between the fibre and ECM stiffness to ensure they are of the same order of magnitude [15]. Here the model is developed using a different implementation of the cellular component (brain grey matter), and has resulted in realistic behaviour when compared to skeletal muscle (Fig 3). Additionally, when a shear stress was applied to the model, the material is able to capture most typical shear behaviour seen in muscle [15, 50]. At small strains there is a linear relationship and little effect from variations in the base material stiffness. At larger strains, there is more nonlinearity in the shear stress-strain relationship and more effect from the base material properties. This demonstrates the nonlinearity in the base material, and is qualitatively similar to the shear results in other muscle models [15]. The order of magnitude of the shear stress is on the same order of magnitude as that of the normal stress, which agrees with the previous findings [50].

Volumetric and strain-energy effects

Skeletal muscles are often viewed as nearly incompressible materials [51], however, volume changes that may occur have often been within the error of the measurement device [46] and recent studies have reported volume changes for long fatiguing contractions [32]. Therefore, the volumetric properties of the model were manipulated to determine the effects of varying the bulk moduli in nearly incompressible materials. Fig 5 demonstrates that variations in the bulk moduli have little effect on the overall stress-strain relationship during passive tests, particularly in the physiological range that muscles typically operate over $\lambda_{\text{muscle}} < 1.1$ [52], which agrees with previous results [53, 54]. This demonstrates that when considering the mechanical behaviour the model there is little dependence on the bulk moduli assuming it is nearly incompressible. [34] suggested that the isochoric and volumetric components of the strain-energy can play a critical role in understanding muscle mechanics on a three dimensional level. When considering the distribution of the strain energy-densities there is an effect from the bulk moduli of the material. The total potential energy in the system, including the energy from activation and external work on the material, is balanced during the quasi-static simulation ran in this study. As the material became more incompressible, the volumetric strain energy-density decreases counteracting the increase in energy seen in the isochoric component of the total strain-energy. The increases in isochoric strain-energy occurred due to increased strain during the passive lengthening phase. These impacts on the energies are likely due to a greater energetic penalty associated with volume change. The isochoric components of the strain energy-density distribution (passive fibre and base material) appear nearly unaffected, which can be

explained by the difference in magnitudes of the strain-energy. However, the distribution of the strain energy-densities was impacted by the choice of bulk moduli, which contributed to the energy balance in muscle and the ability to resist volume change. The total contractile force produced by the muscle during the fixed-end contraction was not strongly impacted by the bulk moduli (Table 2). The main effect from increasing the bulk moduli was in the decreased ability of the material to change volume.

Investigation of the strain-energy distribution in the muscle model allows for an understanding of muscle behaviour during deformation and contraction. Fig 7 shows that as the muscle is pulled to a traction of 1×10^5 Pa there is a strong energy dependence on the stiffness of the material. The results show that there is larger internal energy developed by the material with lower stiffness (2% ECM), which is expected given that compliant tissue will have a larger strain. Interestingly, there are negative volumetric strain energy-densities that appear during passive lengthening and activation. This is due to the calculation of the strain energy-densities, which are calculated with respect to the initial configuration in which the energy is assumed to be zero for all the components. Therefore, negative values are expected for the balance of the energies. The increasing activation in the muscle had a relatively small impact on the passive fibre and base material energies (Fig 7), likely due to the constraints imposed during fixed-length activation restricting movement of the $\pm x$ faces of the geometries. Large variations occur in the volumetric and isochoric energies in Fig 7, and are partly due to the difference in bulk moduli of the micro-mechanical components (similarly to Fig 6). Although, the stiffness of the material does play a significant role in increasing the variation in energy for varying volume fractions. By investigating the effects of the strain energy-density distributions, an understanding of how the stiffness of the material, which can be altered through the homogenized model, impacts the energy lost or gained through a three dimensional muscle architecture. In this case the increase in stiffness of the material was shown to increase the volumetric energies and hence reduce the ability of a muscle to deform or bulge during contraction. This in turn gives an understanding of how the combination of the microscopic composition and macroscopic deformation of the muscle impact the distribution of strain energy-densities, which demonstrates the critical role these material properties play in contributing to the force produced by skeletal muscle. The micro-mechanical parameters demonstrated a strong impact on muscle mechanics, while κ_{cell} had a strong effect on the model's ability to change volume, the volume fraction of the ECM, α , was particularly important in altering the strain energy-density distribution.

Applications

Homogenization models are used to analyze the impacts of the variation of micro-mechanical components, and have the ability to investigate the effects from many conditions such as fibrosis. Fibrosis is the increase in collagen content in the muscle as the result of diseases such as cerebral palsy or muscular dystrophies [22, 28]. This model allows for the investigation of these effects by altering the volume fraction of the ECM. Fig 7 shows that alterations in the volume fraction of the material have strong effects on the mechanics of the muscle, and further investigation of varying micro-mechanical properties and the impacts on the strain energy-density distribution could provide a deeper understanding of the effects from fibrosis. The stiffness parameter for ECM, s_{ECM} , allows for investigation of effects such as glycation, which is a type of biochemical linkage between a sugar and a protein or lipid. In the process of aging, glycation occurs which increases the stiffness of the ECM [55], and these effects could be further understood through an application of this model. The formulation of forces and energies in the model allows for an analysis of the contribution from each of the homogenized

components to the whole muscle mechanics. This ability to analyze the impacts from individual components is not typically found in macroscopic models, but can provide insight into the mechanics of muscles under conditions of varying micro-mechanical properties.

Conclusion

In this paper we have developed a principled model for muscle base material, which has been designed to easily incorporate available micro-mechanical experimental data from the literature into a macroscopic model. The characteristics of this model were then examined through tension and activation experiments for both normal stress and shear stress experiments. The breakdown of the strain energy-densities associated with passive lengthening and activation were analyzed under the effects of micro-mechanical components, and these components were found to have an effect on the distribution of these energies. This numerical model has the potential for gaining a deeper understanding on the effects of changes to the tissue micro-structure and composition on the three dimensional mechanics of muscle contraction.

Supporting information

S1 Appendix. Finite element method description.
(PDF)

Author Contributions

Conceptualization: Ryan N. Konno, Nilima Nigam, James M. Wakeling.

Methodology: Ryan N. Konno, Nilima Nigam, James M. Wakeling.

Software: Ryan N. Konno.

Supervision: Nilima Nigam, James M. Wakeling.

Validation: Ryan N. Konno.

Visualization: Ryan N. Konno.

Writing – original draft: Ryan N. Konno.

Writing – review & editing: Ryan N. Konno, Nilima Nigam, James M. Wakeling.

References

1. Zajac F. Muscle and Tendon: Properties, Models, Scaling, and Application to Biomechanics and Motor Control. *Crit Rev Biomed Eng.* 1989; 17(14):358–410. PMID: [2676342](#)
2. Lieber RL, Fridén J. Functional and Clinical Significance of Skeletal Muscle Architecture. *Muscle Nerve.* 2000; 23(November):1647–1666. [https://doi.org/10.1002/1097-4598\(200011\)23:11%3C1647::AID-MUS1%3E3.0.CO;2-M](https://doi.org/10.1002/1097-4598(200011)23:11%3C1647::AID-MUS1%3E3.0.CO;2-M) PMID: [11054744](#)
3. Randhawa A, Wakeling JM. Multidimensional models for predicting muscle structure and fascicle pennation. *J Theor Biol.* 2015; 382:57–63. <https://doi.org/10.1016/j.jtbi.2015.06.001> PMID: [26073723](#)
4. Rahemi H, Nigam N, Wakeling JM. Regionalizing muscle activity causes changes to the magnitude and direction of the force from whole muscles—a modeling study. *Front Physiol.* 2014; 5 AUG(August):1–10. <https://doi.org/10.3389/fphys.2014.00298> PMID: [25232341](#)
5. Ross SA, Ryan DS, Dominguez S, Nigam N, Wakeling JM. Size, history-dependent, activation and three-dimensional effects on the work and power produced during cyclic muscle contractions. *Integr Comp Biol.* 2018; 58(2):232–250. <https://doi.org/10.1093/icb/icy021> PMID: [29726964](#)
6. Blemker SS, Delp SL. Three-Dimensional Representation of Complex Muscle Architectures and Geometries. *Ann Biomed Eng.* 2005; 33(5):661–673. <https://doi.org/10.1007/s10439-005-1433-7> PMID: [15981866](#)

7. Oomens C, Maenhout M, Van Oijen C, Drost M, Baaijens F. Finite element modelling of contracting skeletal muscle. *Philos Trans R Soc Lond, B, Biol Sci.* 2003; 358(1437):1453–1460. <https://doi.org/10.1098/rstb.2003.1345> PMID: 14561336
8. Yucesoy CA, Koopman BH, Huijting PA, Grootenboer HJ. Three-dimensional finite element modeling of skeletal muscle using a two-domain approach: linked fiber-matrix mesh model. *J Biomech.* 2002; 35(9):1253–1262. [https://doi.org/10.1016/S0021-9290\(02\)00069-6](https://doi.org/10.1016/S0021-9290(02)00069-6) PMID: 12163314
9. Weiss JA, Maker BN, Govindjee S. Finite element implementation of incompressible, transversely isotropic hyperelasticity. *Comput Method Appl M.* 1996; 135(1-2):107–128. [https://doi.org/10.1016/0045-7825\(96\)01035-3](https://doi.org/10.1016/0045-7825(96)01035-3)
10. Sharafi B, Blemker SS. A micromechanical model of skeletal muscle to explore the effects of fiber and fascicle geometry. *J Biomech.* 2010; 43(16):3207–3213. <https://doi.org/10.1016/j.jbiomech.2010.07.020> PMID: 20846654
11. Virgilio KM, Martin KS, Peirce SM, Blemker SS. Multiscale models of skeletal muscle reveal the complex effects of muscular dystrophy on tissue mechanics and damage susceptibility. *Interface Focus.* 2015; 5(2). <https://doi.org/10.1098/rsfs.2014.0080> PMID: 25844152
12. Ceelen KK, Oomens CWJ, Baaijens FPT. Microstructural analysis of deformation-induced hypoxic damage in skeletal muscle. *Biomech Model Mechanobiol.* 2008; 7(4):277–284. <https://doi.org/10.1007/s10237-007-0097-7> PMID: 17710456
13. Röhrle O, Davidson JB, Pullan AJ. A physiologically based, multi-scale model of skeletal muscle structure and function. *Front Physiol.* 2012; 3 SEP(September):1–14. <https://doi.org/10.3389/fphys.2012.00358> PMID: 22993509
14. Böl M, Reese S. Micromechanical modelling of skeletal muscles based on the finite element method. *Comput Method Biomech.* 2008; 11(5):489–504. <https://doi.org/10.1080/10255840701771750> PMID: 19230146
15. Spyrou LAA, Agoras M, Danas K. A homogenization model of the Voigt type for skeletal muscle. *J Theor Biol.* 2017; 414(July 2016):50–61. <https://doi.org/10.1016/j.jtbi.2016.11.018> PMID: 27884495
16. Spyrou LA, Brisard S, Danas K. Multiscale modeling of skeletal muscle tissues based on analytical and numerical homogenization. *J Mech Behav Biomed.* 2019; 92:97–117. <https://doi.org/10.1016/j.jmbbm.2018.12.030> PMID: 30677705
17. Bleiler C, Ponte Castañeda P, Röhrle O. A microstructurally-based, multi-scale, continuum-mechanical model for the passive behaviour of skeletal muscle tissue. *J Mech Behav Biomed.* 2019; 97(April):171–186. <https://doi.org/10.1016/j.jmbbm.2019.05.012> PMID: 31125890
18. Gillies AR, Lieber RL. Structure and function of the skeletal muscle extracellular matrix. *Muscle Nerve.* 2011; 44(3):318–331. <https://doi.org/10.1002/mus.22094> PMID: 21949456
19. Purslow PP. Strain-induced reorientation of an intramuscular connective tissue network: Implications for passive muscle elasticity. *J Biomech.* 1989; 22(1):21–31. [https://doi.org/10.1016/0021-9290\(89\)90181-4](https://doi.org/10.1016/0021-9290(89)90181-4) PMID: 2914969
20. Binder-Markey BI, Broda NM, Lieber RL. Intramuscular anatomy drives collagen content variation within and between muscles. *Front Physiol.* 2020; 11:293. <https://doi.org/10.3389/fphys.2020.00293> PMID: 32362834
21. Lieber RL, Runesson E, Einarsson F, Fridén J. Inferior mechanical properties of spastic muscle bundles due to hypertrophic but compromised extracellular matrix material. *Muscle Nerve.* 2003; 28(4):464–471. <https://doi.org/10.1002/mus.10446> PMID: 14506719
22. Lieber RL, Ward SR. Cellular mechanisms of tissue fibrosis. 4. structural and functional consequences of skeletal muscle fibrosis. *Am J Physiol Cell Physiol.* 2013; 305(3). <https://doi.org/10.1152/ajpcell.00173.2013> PMID: 23761627
23. Sleboda DA, Stover KK, Roberts TJ. Diversity of extracellular matrix morphology in vertebrate skeletal muscle. *J Morphol.* 2020; 281(2):160–169. <https://doi.org/10.1002/jmor.21088> PMID: 31840868
24. Turrina A, Martínez-González MA, Stecco C. The muscular force transmission system: Role of the intramuscular connective tissue. *J Bodyw Mov Ther.* 2013; 17(1):95–102. <https://doi.org/10.1016/j.jbmt.2012.06.001> PMID: 23294690
25. Mayne R, Sanderson RD. The Extracellular Matrix of Skeletal Muscle. *Top Catal.* 1985; 5(5):449–468. [https://doi.org/10.1016/S0174-173X\(85\)80032-7](https://doi.org/10.1016/S0174-173X(85)80032-7) PMID: 3910337
26. Purslow PP. The structure and functional significance of variations in the connective tissue within muscle. *Comp Biochem Physiol Part A Mol Integr Physiol.* 2002; 133(4):947–966. [https://doi.org/10.1016/S1095-6433\(02\)00141-1](https://doi.org/10.1016/S1095-6433(02)00141-1) PMID: 12485685
27. Trotter JA, Richmond FJ, Purslow PP. Functional morphology and motor control of series-fibered muscles. *Exerc Sport Sci Rev.* 1995; 23:167–213. <https://doi.org/10.1249/00003677-199500230-00008> PMID: 7556350

28. Smith LR, Lee KS, Ward SR, Chambers HG, Lieber RL. Hamstring contractures in children with spastic cerebral palsy result from a stiffer extracellular matrix and increased in vivo sarcomere length. *J Physiol*. 2011; 589(10):2625–2639. <https://doi.org/10.1113/jphysiol.2010.203364> PMID: 21486759
29. Yeoh OH. Some Forms of the Strain Energy Function for Rubber. *Rubber Chem Technol*. 1993; 66(5):754–771. <https://doi.org/10.5254/1.3538343>
30. Jin X, Zhu F, Mao H, Shen M, Yang KH. A comprehensive experimental study on material properties of human brain tissue. *J Biomech*. 2013; 46(16):2795–2801. <https://doi.org/10.1016/j.jbiomech.2013.09.001> PMID: 24112782
31. Prange MT, Margulies SS. Regional, directional, and age-dependent properties of the brain undergoing large deformation. *J Biomech Eng*. 2002; 124(2):244–252. <https://doi.org/10.1115/1.1449907> PMID: 12002135
32. Willwacher S, Sleboda DA, Mählich D, Brüggemann GP, Roberts TJ, Bratke G. The time course of calf muscle fluid volume during prolonged running. *Physiol Rep*. 2020; 8(9). <https://doi.org/10.14814/phy2.14414> PMID: 32378332
33. Sleboda DA, Wold ES, Roberts TJ. Passive muscle tension increases in proportion to intramuscular fluid volume. *J Exp Biol*. 2019; 222(21):jeb209668. <https://doi.org/10.1242/jeb.209668> PMID: 31558592
34. Wakeling JM, Ross SA, Ryan DS, Bolsterlee B, Konno R, Domínguez S, et al. The Energy of Muscle Contraction. I. Tissue Force and Deformation During Fixed-End Contractions. *Front Physiol*. 2020; 11. <https://doi.org/10.3389/fphys.2020.00813> PMID: 32982762
35. Simo JC, Taylor RL. Quasi-incompressible finite elasticity in principal stretches. continuum basis and numerical algorithms. *Comput Method Appl M*. 1991; 85(3):273–310. [https://doi.org/10.1016/0045-7825\(91\)90100-K](https://doi.org/10.1016/0045-7825(91)90100-K)
36. Arndt D, Bangerth W, Davydov D, Heister T, Heltai L, Kronbichler M, et al. The deal.II Library, Version 8.5. *J Numer Math*. 2017; 25:137–146. <https://doi.org/10.1515/jnma-2017-0058>
37. Domínguez S. From eigenbeauty to large-deformation horror. Ph.D. Thesis, Simon Fraser University. 2020. Available from: <http://summit.sfu.ca/item/20968>
38. Simo JC, Miehe C. Associative coupled thermoplasticity at finite strains: Formulation, numerical analysis and implementation. *Comput Method Appl M*. 1992; 98(1):41–104. [https://doi.org/10.1016/0045-7825\(92\)90170-O](https://doi.org/10.1016/0045-7825(92)90170-O)
39. Gillies AR, Smith LR, Lieber RL, Varghese S. Method for decellularizing skeletal muscle without detergents or proteolytic enzymes. *Tissue Eng Part C Methods*. 2011; 17(4):383–389. <https://doi.org/10.1089/ten.tec.2010.0438> PMID: 20973753
40. Böll M, Iyer R, Dittmann J, Garcés-Schröder M, Dietzel A. Investigating the passive mechanical behaviour of skeletal muscle fibres: Micromechanical experiments and Bayesian hierarchical modelling. *Acta Biomater*. 2019; 92:277–289. <https://doi.org/10.1016/j.actbio.2019.05.015> PMID: 31077887
41. Budday S, Sommer G, Birkl C, Langkammer C, Haybaeck J, Kohnert J, et al. Mechanical characterization of human brain tissue. *Acta Biomater*. 2017; 48:319–340. <https://doi.org/10.1016/j.actbio.2016.10.036> PMID: 27989920
42. Karimi A, Shojaei A. An Experimental Study to Measure the Mechanical Properties of the Human Liver. *Digest Dis*. 2018; 36(2):150–155. <https://doi.org/10.1159/000481344> PMID: 29131053
43. Chui C, Kobayashi E, Chen X, Hisada T, Sakuma I. Combined compression and elongation experiments and non-linear modelling of liver tissue for surgical simulation. *Med Biol Eng Comput*. 2004; 42(6):787–798. <https://doi.org/10.1007/BF02345212> PMID: 15587470
44. Mohammadkhah M, Murphy P, Simms CK. The in vitro passive elastic response of chicken pectoralis muscle to applied tensile and compressive deformation. *J Mech Behav Biomed*. 2016; 62:468–480. <https://doi.org/10.1016/j.jmbbm.2016.05.021> PMID: 27281164
45. Winters TM, Takahashi M, Lieber RL, Ward SR. Whole muscle length-tension relationships are accurately modeled as scaled sarcomeres in rabbit hindlimb muscles. *J Biomech*. 2011; 44(1):109–115. <https://doi.org/10.1016/j.jbiomech.2010.08.033> PMID: 20889156
46. Bolsterlee B, D'Souza A, Gandevia SC, Herbert RD. How does passive lengthening change the architecture of the human medial gastrocnemius muscle? *J Appl Physiol*. 2017; 122(4):727–738. <https://doi.org/10.1152/jappphysiol.00976.2016> PMID: 28104754
47. Van Loocke M, Simms CK, Lyons CG. Viscoelastic properties of passive skeletal muscle in compression-cyclic behaviour. *J Biomech*. 2009; 42(8):1038–48. <https://doi.org/10.1016/j.jbiomech.2009.02.022> PMID: 19368927
48. Takaza M, Moerman KM, Gindre J, Lyons G, Simms CK. The anisotropic mechanical behaviour of passive skeletal muscle tissue subjected to large tensile strain. *J Mech Behav Biomed*. 2013; 17:209–220. <https://doi.org/10.1016/j.jmbbm.2012.09.001> PMID: 23127635

49. Fine RA, Millero FJ. Compressibility of water as a function of temperature and pressure. *J Chem Phys.* 1973; 59(10):5529–5536. <https://doi.org/10.1063/1.1679903>
50. Sharafi B, Blemker SS. A mathematical model of force transmission from intrafascicularly terminating muscle fibers. *J Biomech.* 2011; 44(11):2031–2039. <https://doi.org/10.1016/j.jbiomech.2011.04.038> PMID: 21676398
51. Abbott BC, Baskin RJ. Volume changes in frog muscle during contraction. *J Physiol.* 1962; 161(3):379–391. <https://doi.org/10.1113/jphysiol.1962.sp006893> PMID: 13858824
52. Maganaris CN. Force-length characteristics of in vivo human skeletal muscle. *Acta Physiol Scand.* 2001; 172(4):279–285. <https://doi.org/10.1046/j.1365-201x.2001.00799.x> PMID: 11531649
53. Pierrat B, Murphy JG, MacManus DB, Gilchrist MD. Finite element implementation of a new model of slight compressibility for transversely isotropic materials. *Comput Method Biomech.* 2016; 19(7):745–758. <https://doi.org/10.1080/10255842.2015.1061513> PMID: 26252069
54. Gardiner JC, Weiss JA. Simple shear testing of parallel-fibered planar soft tissues. *J Biomech Eng.* 2001; 123(2):170–175. <https://doi.org/10.1115/1.1351891> PMID: 11340878
55. Haus JM, Carrithers JA, Trappe SW, Trappe TA. Collagen, cross-linking, and advanced glycation end products in aging human skeletal muscle. *J Appl Physiol.* 2007; 103(6):2068–2076. <https://doi.org/10.1152/jappphysiol.00670.2007> PMID: 17901242